Heliyon 5 (2019) e02040

Contents lists available at ScienceDirect

Heliyon

journal homepage: www.heliyon.com

Numerical integration strategies of PFR dynamic models with axial dispersion and variable superficial velocity: the case of CO_2 capture by a solid sorbent

A. Di Giuliano *, E. Pellegrino

University of L'Aquila, Department of Industrial and Computer Engineering and Economics, 18 via G. Gronchi, 67100, L'Aquila, Italy

ARTICLE INFO

Keywords:
Chemical engineering
CO_2 capture modelling
Particle grain model
Axial dispersion plug flow reactor model
Method of lines
Variable superficial velocity

ABSTRACT

In order to integrate mole balances (partial differential equations) of an Axial Dispersion Plug Flow Reactor (ADPFR) model, the overall superficial velocity is usually considered constant, a hypothesis which fits well only null or negligible variations of volumetric flow rate, e.g. feeding flow strongly diluted by inert species. This work proposes a numerical-integration approach (based on the method of lines) for ADPFR dynamic modelling, applied to simulate the CO_2 capture in an isothermal-isobaric packed bed, made of purposely synthesized and experimentally characterized CaO-mayenite sorbent particles. This approach proved to be suitable for both constant and variable superficial velocity with respect to time and space. With the latter option, velocity profiles agreed with simulated reactive phenomena, while discrepancies between solutions from the two options became increasingly evident as dilution of inlet CO_2 decreased. N_2 flow rate and CO_2 mole balances obtained from numerical-integrations with variable superficial velocity appeared as the most physicochemically reasonable.

1. Introduction

In chemical reactors engineering, the introduction of axial dispersion is a recognized tool to implement real flow conditions in an ideal Plug Flow Reactor (PFR) model, which assumes fluid molecules to have a flat velocity profile at any given position along the tubular reactor axis, i.e. no element of fluid overtakes or mixes with any other element ahead or behind [1, 2, 3]. Nonideality brought in by axial dispersion consists of considering mixing and diffusion within the fluid, along the axial direction: eddies and slippage occur a considerable number of times while fluid flows through the reactor, therefore these disturbances with respect to ideal plug flow may be considered as statistical in nature, somewhat as in molecular diffusion [3]. In the resulting Axial Dispersion Plug Flow Reactor (ADPFR) model, for each fluid species i, axial dispersion is superimposed on its bulk flow $u{\cdot}S{\cdot}C_i$, by a form in analogy with Fick's law for molecular diffusion $-D_R(\partial C_i/\partial z){\cdot}S$ (see Table 1 for the menaning of symbols used in this paper) [1, 2, 3]. The resulting molar flow rate of i in an ADPFR is defined as in Eq. (1) [1].

$$F_i = S\left[- D_R\frac{\partial C_i}{\partial z} + uC_i\right] \tag{1}$$

Concentration profiles inside a PFR and an ADPFR are compared in Fig. 1: in the former (Fig. 1 a), at a given axial position each molecule moves exactly at the same velocity, developing a flat front on cross-sectional area S (i.e. the plug flow); in the latter (Fig. 1 b), some molecules jump forward, ahead of the molar average velocity front, while others lag behind, developing a non-uniform actual velocity front on S [1].

When Eq. (1) is introduced in the dynamic mole balance for i in a tubular reactor – in which i reacts with the rate $\boldsymbol{r_i}$ – Eq. (2) is obtained, defining the general ADPFR mole balance in unsteady state:

$$\frac{\partial C_i}{\partial t} = D_R\frac{\partial^2 C_i}{\partial z^2} - \frac{\partial(uC_i)}{\partial z} + \boldsymbol{r_i} \tag{2}$$

In Eq. (2), both factors in the first-order derivative with respect to z are functions of z and t, in principle. Nonetheless, as often done in chemical reaction engineering textbooks [1, 3], the implicit assumption

* Corresponding author.
E-mail address: andrea.digiuliano@univaq.it (A. Di Giuliano).

https://doi.org/10.1016/j.heliyon.2019.e02040
Received 26 March 2019; Received in revised form 30 May 2019; Accepted 1 July 2019

Table 1
Notation.

Acronyms	
ADPFR	Axial Dispersion Plug Flow Reactor
BC	Boundary Condition(s)
CBN	Carbonation
CSCM	Combined Sorbent-Catalyst Material(s)
IC	Initial Condition(s)
ICDD	International Centre of Diffraction Data
MOL	Method Of Lines
ODE	Ordinary Differential Equation(s)
PDE	Partial Differential Equation(s)
PDF	Powder Diffraction Files data
PFR	Plug Flow Reactor
PGM	Particle Grain Model
SESMR	Sorption-Enhanced Steam Methane Reforming
TGA	Thermo-Gravimetric Analysis
XRD	X-Ray Diffraction
Symbols	
a	parameter in Equation 15, dimensionless
b	parameter in Equation 15, dimensionless
C	molar concentration, kmol m^{-3}
$C(K)$	constant coefficients defined in Table 3 with $(K) = 1, 2, 3, 4, 5$
D	molecular diffusion coefficient, $m^2\ s^{-1}$
d_p	particle diameter, m
D_{PL}	product layer diffusivity coefficient, $m^2\ s^{-1}$
D_R	axial dispersion coefficient, $m^2\ s^{-1}$
D_{Knu}	Knudsen diffusivity, $m^2\ s^{-1}$
F	molar flow rate, kmol s^{-1}
h	mass transfer coefficient, m s^{-1}
H	height of the active packed bed, m
I	number of discretized steps in t^*, dimensionless
J	number of discretized steps in z^* direction, dimensionless
k_S	kinetic constant for surface reaction, $m^4\ kmol^{-1}\ s^{-1}$
m	mass, kg
M	molecular weight, kg $kmol^{-1}$
n_{CaO}	CaO moles per unit particle volume, kmol m^{-3}
$O(x^k)$	error of order k with respect to the variable x
P	pressure, atm
R	particle radius, m
$\mathscr{R}$	ideal gas constant, kJ $kmol^{-1}\ K^{-1}$
r	particle radial coordinate, m
r	rate of reaction, kmol $m^3\ s^{-1}$
S	reactor cross-sectional area, m^2
T	temperature, K
t	time, s
u	superficial velocity, m s^{-1}
v	molar volume, $m^3\ kmol^{-1}$
V	overall volume, m^3
w	weight fraction, dimensionless
X	sorbent conversion, dimensionless
y	molar fraction, dimensionless
z	reactor axial coordinate, m
Greek letters	
α	parameter in Equation 14, dimensionless
Γ	sorption capacity, $g_{CO2}\ g_{\text{calcined material}}^{-1}$
Δ	difference
δ_{CaO}	CaO grain diameter, m
ε	packed bed void fraction, dimensionless
ε_p	internal particle void fraction, dimensionless
ζ	$CaCO_3$/CaO molar volumes ratio, dimensionless
ρ	density, kg m^{-3}
σ_{CaO}	CaO grain surface per unit of particle volume, m^{-1}
τ	characteristic time, s
Subscripts and superscripts	
(i)	progressive index of discretized steps on z^*
0	initial
b	packed bed
CaO	calcium oxide
eff	effective
eq	equilibrium
fin	final
i	generic chemical species
in	inlet
(j)	progressive index of discretized steps on t^*
out	outlet
p	particle
tot	total
$*$	dimensionless

is considered of constant superficial velocity, obtaining Eq. (3):

$$\frac{\partial C_i}{\partial t} = D_R \frac{\partial^2 C_i}{\partial z^2} - u\frac{\partial C_i}{\partial z} + \boldsymbol{r_i} \tag{3}$$

This simplified form of ADPFR mole balance (Eq. (3)) usually appears in modelling studies for tubular reactors [1, 3, 4, 5, 6, 7] or fluidized beds reactors (especially in two-phase modelling of turbulent fluidization) [8, 9, 10, 11, 12, 13, 14, 15]. However, even at constant temperature and pressure, when chemical reactions cause an overall variation of molar flow, as far as gaseous media are concerned, applicability of Eq. (3) is limited to reacting species i sufficiently diluted in inert gases; in fact, the overall molar flow rate and superficial velocity do not vary markedly in these conditions, independently on species i conversion. This could not be the case of industrial reactors, where reactants dilution may be avoided so to contain operating and construction costs. A similar issue was posed in studies about non-isothermal and non-isobaric fluidized bed industrial reactors, considering the variations of the overall superficial velocity along the reactor height, which can influence fluidization quality [16].

These observations pose an interesting problem about modelling of chemical reactors, since the mathematical differences between ADPFR mole balances which consider (Eq. (2)) or not (Eq. (3)) a variable superficial velocity may determine the success or failure of a given numerical-integration method, when applied to the related model. Froment [17], in his relevant study about modelling of packed bed reactors, had already referred as a serious problem the numerical integration of nonlinear, second-order Partial Differential Equations (PDE) as Eqs. (2) and (3), because of mathematical stability of the solution [17]. To the best of our knowledge, the issue of ADPFR modelling with variable superficial velocity is just mentioned in well-spread, even recent chemical reaction engineering textbooks [1, 2, 3], without the bridging approach used in this work towards numerical applications. In fact, we aimed to contribute to fill this gap, considering the applicability of a numerical-integration method for an ADPFR model with the generalized form of the mole balance on gaseous species i (Eq. (2)), as well as with its form involving constant superficial gas velocity (Eq. (3)).

The chosen case of study is the CO_2 capture from a N_2/CO_2 stream by carbonation of CaO (Reaction 1), in a packed bed reactor filled with a granular CaO-mayenite sorbent, actually synthesized and characterized; this case is suitable to test the influence of a variable superficial velocity, as it deals with an unsteady state process in which a gas-solid reaction causes a decrease of gaseous flow rate:

$$\text{CBN: } CaO_{(s)} + CO_{2(g)} \leftrightarrow CaCO_{3(s)}\ \Delta H^0_{298\ K} = -175.7\ \text{kJ mol}^{-1}\ \text{Reaction 1}$$

Previous publications described the development and validation of a Particle Grain Model (PGM) to simulate CO_2-capture within porous particles of a CaO-based sorbent [6, 7, 18, 19], and of an ADPFR dynamic model to simulate Sorption Enhanced Steam Methane Reforming (SESMR) in a bench scale packed bed made of combined sorbent-catalyst bifunctional particles [6, 7]. The assumption of constant gas superficial velocity was made in [6, 7], justified by a large fraction of inert species in the gas mixture flowing through the reactor in those laboratory tests, and numerical-integration of the resulting ADPFR dynamic model was performed by "pdepe" tool in MATLAB® [6, 7], developed for parabolic-elliptic PDE in one dimension [20].

In this work, a different numerical-integration approach is proposed, since the ADPFR model with superficial velocity as unknown, dependent

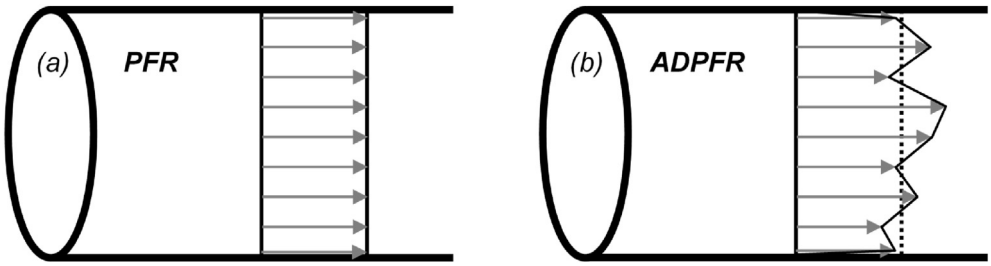

Fig. 1. Representation of concentration profiles within a fluid flowing through a tubular reactor: (a) PFR case; (b) ADPFR case.

function contains PDE with more complex mathematical features: an ad hoc routine was developed in MATLAB®, based on the Method Of Lines (MOL) [21]. The structure of ADPFR model and the application of MOL are fully described in Section 3, commenting both successful and unsuccessful numerical-integrations implemented in MATLAB®;. The working integration algorithm based on MOL is presented (Section 3), proving that it works with and without the hypothesis of constant superficial velocity by simulations for the chosen case of study (Section 4). Further insights into physicochemical effects brought about by assumptions on superficial velocity are provided (Section 4), by comparing three process quantities at different inlet CO_2 concentrations: outlet CO_2 concentration, outlet inert flow rate and overall cumulative CO_2 mole balance.

2. Materials and methods

2.1. Description of the case of study

The case of study assumed to apply the numerical-integration method for the ADPFR dynamic model is the CO_2 capture from a N_2/CO_2 stream. The test rig and process conditions are those described in [6, 22]: the packed bed reactor has an internal diameter of 7 mm, contains 0.5 g of particles with diameters in the range 100–125 μm, is fed with 20 Nml min^{-1} of a mixture of CO_2 in N_2. The process occurs at constant pressure and temperature: 1 atm and 650 °C, respectively.

2.2. Experimental methods

An actual CaO-mayenite material – synthesized by the wet mixing method validated in [23, 24] – was assumed as the CO_2 sorbent of the ADPFR modelling study. From here on, this material is named CaOMAY.

All the physicochemical properties needed as inputs for the modelling study were experimentally measured. Particle density and porosity (i.e. void fraction) of the calcined sorbent were determined by GEOPYC 1360 and ACCUPYC 1330 devices, respectively, as done in [7]. Crystalline phases were identified by X-Ray Diffraction (XRD) and crystallites average dimensions of detected phases were estimated by Scherrer equation [23, 25, 26], according to methods fully described elsewhere [23].

A long-term CO_2 capture test was carried out on CaOMAY by Thermo-Gravimetric Analysis (TGA) measurements, according to the same method and by means of the same device described in [27] (capture conditions: 1 atm, 650 °C, 15 vol% CO_2 in N_2): sample mass variation ($\Delta m(t)$) with respect to totally calcined sample mass (m^0) was recorded during the whole test duration (7 h), so to determine actual maximum sorption capacity of CaOMAY ($\Gamma = \Delta m(7\ h)/m^0$) and the related CaO conversion as a function of time ($X = \Delta m(t)/(\Gamma\ m^0)$).

2.3. Carbonation kinetics and TGA data fitting by PGM

The PGM detailed by Di Giuliano et al. [7] (Table 2), deriving from [6, 7, 18, 19], was used in this work to interpret the behaviour of CaOMAY with regard to carbonation (Reaction 1), on the basis of TGA experimental data.

The PGM is based on the following considerations: (i) the sorbent particle is pictured as an aggregate of spherical grains made of inert (mayenite) or sorbent (CaO) materials, with interstitial voids constituting the particle porosity (ε_p^0); (ii) each of these particles is exposed to a stagnant CO_2/N_2 atmosphere (Eq. (6)), with CO_2 moving through particle pores by diffusion (Eqs. (5), (14)); (iii) CO_2 reacts with CaO at the sorbent grain surface (Eq. (4)), so that a shell of $CaCO_3$ grows on that shrinking core of CaO; (iv) this product layer, becoming progressively more thick and compact as CaO conversion increases, is penetrated with greater resistance by CO_2 directed towards the reacting surface of CaO shrinking core (Eq. (15)); (v) internal porosity decreases as the CaO conversion increases, because of the ratio of $CaCO_3$ molar volume to CaO one ($\zeta = 2.18$ in Eq. (7)). By virtue of these hypotheses, the whole sorption mechanism is modelled by the shrinking core approach applied to CaO grains, according to the first-order surface reaction kinetics by Bhatia and Perlmutter [28] and with a product layer diffusion coefficient decreasing exponentially as a function of CaO conversion (Eq. (15)) [18]; the resulting rate for carbonation (Reaction 1) is defined in Eq. (13) [7].

More in detail, the PGM described in Table 2 was used in order to find values of parameters a, b and δ_{CaO}^0 (Eq. (13), (15)), able to make the PGM output fit faithfully the experimental carbonation data from CaOMAY TGA test, both expressed as CaO conversion as a function of time (X). On the basis of findings and experimental validations from Di Giuliano et al. [7] and Aloisi et al. [6], these parameters can be reasonably used to simulate the behaviour of CaOMAY in an ADPFR carrying out carbonation (Reaction 1).

Values of a, b and δ_{CaO}^0, together with data from experimental characterization described in Section 2.2, complete the information set needed to describe CaOMAY in the ADPFR dynamic reactor model.

3. Model

As far as a steady state PFR with gaseous species is concerned, the usual approach to compile mole balances consists of using molar flow rates F_i as unknown functions of z and t [1].

With ADPFR modelling, because of the definition of F_i in Eq. (1) and under the hypothesis of unsteady state, molar concentrations C_i necessarily appear as unknown functions in second-order PDE: their substitution with the term $(F_i/F_{tot})\cdot(P/\mathscr{R}T)$ does not result in a simplifying method to rewrite Eq. (2) or Eq. (3), especially when multiple reactions are concerned. Therefore, the set of C_i is the most convenient choice to represent chemical species as unknown functions in the formulation of an ADPFR dynamic model, with the addition of variable superficial velocity u when the more general Eq. (2) is considered.

The CO_2 capture case of study, described in Section 2.1, was modelled according to considerations just above. For particles in the packed bed, dependencies on z and t of CaO dynamic conversion (X) and consequent evolution of particles void fraction (ε_p) were expressed by Eqs. (4) and (7), respectively. With regard to the gas phase inside the

Table 2
PGM equations, initial conditions, boundary conditions and dimensionless variables [7].

$\frac{\partial X}{\partial t} = \frac{r_{CBN}}{n^0_{CaO}}$	Mole balance on sorbent phase (CaO)	(4)
$\frac{\partial(\varepsilon_p \cdot C_{CO_2})}{\partial t} = \frac{1}{r^2}\frac{\partial}{\partial r}\left(D_{CO_2,eff}\, r^2 \frac{\partial C_{CO_2}}{\partial r}\right) - r_{CBN}$	Mole balance on CO_2 within ε_p	(5)
$C_{N_2} = C_{tot} - C_{CO_2} = \frac{P}{\mathscr{R}T} - C_{CO_2}$	Congruence on inert gas (N_2)	(6)
$\frac{\partial \varepsilon_p}{\partial t} = -(\zeta - 1)\nu_{CaO}\, n^0_{CaO}\frac{\partial X}{\partial t}$	Dynamic evolution of ε_p due to CBN	(7)
Initial conditions (IC):		
$X(0 \le r \le R_p,\ t = 0) = 0$	Completely calcined particle	(8)
$C_{N_2}(0 \le r \le R_p, t = 0) = C_{tot} = \frac{P}{\mathscr{R}T}$	ε_p filled by inert	(9)
Boundary conditions (BC), $\forall\, t > 0$:		
$\left.\frac{\partial C_{CO_2}}{\partial r}\right\|_{r=0} = 0$	Radial symmetry of concentration profiles	(10)
$D_{CO_2,eff}\left.\frac{\partial C_{CO_2}}{\partial r}\right\|_{r=R_p} = h_{CO_2} \cdot (C_{CO_2,bulk} - C_{CO_2}(r = R_p))$	No accumulation on particle external borders	(11)
where:		
$X = X(r,t);\ C_{CO_2} = C_{CO_2}(r,t);\ \varepsilon_p = \varepsilon_p(r,t)$	Functions of time (t) and particle radius (r)	(12)
$r_{CBN} = \frac{k_s n^0_{CaO}\sigma^0_{CaO}(1-X)^{2/3}(C_{CO_2} - C_{CO_2,eq})}{1 + \frac{k_s n^0_{CaO}}{2 D_{PL}}\delta^0_{CaO}\sqrt[3]{1-X}\left(1 - \sqrt[3]{\frac{1-X}{1-X+\zeta X}}\right)}$	CBN kinetic law	(13)
$D_{CO_2,eff} = \frac{1}{(1 - y_{CO_2})/D_{CO_2,N_2} + 1/D_{Knu,CO_2}}\varepsilon_p{}^{\alpha}$	CO_2 effective diffusivity within ε_p	(14)
$D_{PL} = D_{PL,0}\exp(-aX^b)$	CO_2 diffusivity through $CaCO_3$ layer	(15)
The above conservation equations, congruence, boundary and initial conditions are made dimensionless by introducing the following variables:		
$y_{CO_2} = C_{CO_2}\frac{\mathscr{R}T}{P},\ r^* = \frac{r}{R},\ t^* = \frac{t}{\tau_{CBN}}$ with $\tau_{CBN} = \frac{\delta^0_{CaO}}{k_s \cdot n^0_{CaO}}$	Dimensionless variables	
The dimensionless system of equations is integrated numerically by the MATLAB® "pdepe" algorithm.		

entire void volume of the packed bed (i.e. packed bed void faction ε plus internal particles void fraction $(1-\varepsilon)\varepsilon_p$), the mole balance on CO_2 was compiled on the basis of Eq. (2) (superficial velocity as a function of z and t) or Eq. (3) (constant superficial velocity); from here on, the former option is called ADPFRu(z,t), the latter is labelled as ADPFRu(const).

Intraparticle diffusive phenomena were negligible in the examined case (packed bed made of fine sorbent particles), so that CO_2 concentration on the sorbent grain surface in Eq. (13) was assumed to be the same as that in the approaching gaseous phase and uniform inside the particle (its change with particle radius, Eq. (5), was neglected).

3.1. Development of ADPFRu(z,t) numerical-integration

Table 3 summarizes the whole set of equations, initial and boundary conditions associated with the ADPFRu(z,t) option.

Eq. (2) was used to represent the heterogeneous gas/solid Reaction 1, occurring inside the packed bed reactor between flowing CO_2 and porous particles of CaOMAY; Eq. (16) resulted, i.e. the mole balance for CO_2 in

Table 3
ADPFRu(z,t) and ADPFRu(const) equations, initial conditions, boundary conditions and dimensionless variables.

	ADPFRu(z,t)		ADPFRu(const)	
ADPFR mole balance on CO_2 in ε and ε_p	$\frac{\partial}{\partial t}\{(\varepsilon + (1-\varepsilon)\varepsilon_p)C_{CO_2}\} = D_R\frac{\partial^2 C_{CO_2}}{\partial z^2} - u\frac{\partial C_{CO_2}}{\partial z} - C_{CO_2}\frac{\partial u}{\partial z} - r_{CBN}(1-\varepsilon)$	(16)	$\frac{\partial}{\partial t}\{(\varepsilon + (1-\varepsilon)\varepsilon_p)C_{CO_2}\} = D_R\frac{\partial^2 C_{CO_2}}{\partial z^2} - u\frac{\partial C_{CO_2}}{\partial z} - r_{CBN}(1-\varepsilon)$	(17)
Overall ADPFR mole balance on gas in ε and ε_p	$\frac{\partial u}{\partial z} = -r_{CBN}\frac{(1-\varepsilon)}{C_{tot}} - (1-\varepsilon)\frac{\partial \varepsilon_p}{\partial t}$	(18)	$u(z,t) = u_{in} = \frac{F_{in,tot}}{C_{tot}\, S} = constant$	(19)
CaO dynamic conversion	$\frac{\partial X}{\partial t} = \frac{r_{CBN}}{n^0_{CaO}}$	(4)	$\frac{\partial X}{\partial t} = \frac{r_{CBN}}{n^0_{CaO}}$	(4)
Dynamic evolution of ε_p due to CBN	$\frac{\partial \varepsilon_p}{\partial t} = -(\zeta - 1)\nu_{CaO}\, n^0_{CaO}\frac{\partial X}{\partial t}$	(7)	$\frac{\partial \varepsilon_p}{\partial t} = -(\zeta - 1)\nu_{CaO}\, n^0_{CaO}\frac{\partial X}{\partial t}$	(7)
	Initial conditions (IC):		Initial conditions (IC):	
Completely calcined particle	$X(0 \le z \le H,\ t = 0) = 0$	(20)	$X(0 \le z \le H,\ t = 0) = 0$	(20)
ε and ε_p filled by inert	$C_{N_2}(0 \le z \le H, t = 0) = C_{tot} = \frac{P}{\mathscr{R}T}$	(21)	$C_{N_2}(0 \le z \le H, t = 0) = C_{tot} = \frac{P}{\mathscr{R}T}$	(21)
Inert molar flow equal to inlet process one	$u(0 \le z \le H, t = 0) = u_{in} = \frac{F_{in,tot}}{C_{tot}\, S}$	(22)	/	
	Boundary conditions (BC), $\forall\, t^* > 0$:		Boundary conditions (BC), $\forall\, t^* > 0$:	
Danckwerts closed-closed vessel boundary conditions [1]	$F_{CO_2,in} = S\, u_{in}C_{CO_2,in} = S\left(uC_{CO_2} - D_R\frac{\partial C_{CO_2}}{\partial z}\right)\Big\|_{z=0}$; $\left.\frac{\partial C_{CO_2}}{\partial z}\right\|_{z=H} = 0$	(23)	$F_{CO_2,in} = S\, u_{in}C_{CO_2,in} = S\left(u_{in}C_{CO_2} - D_R\frac{\partial C_{CO_2}}{\partial z}\right)\Big\|_{z=0}$; $\left.\frac{\partial C_{CO_2}}{\partial z}\right\|_{z=H} = 0$	(24)
Left boundary condition on u	$u(z = 0, t) = u_{in} = \frac{F_{in,tot}}{C_{tot}\, S}$	(25)	/	
Unknown functions:	$X = X(z,t)\ ;\ C_{CO_2} = C_{CO_2}(z,t)\ ;\ \varepsilon_p = \varepsilon_p(z,t)\ ;\ u = u(z,t)$		$X = X(z,t)\ ;\ C_{CO_2} = C_{CO_2}(z,t)\ ;\ \varepsilon_p = \varepsilon_p(z,t)$	
The above conservation equations, boundary and initial conditions are made dimensionless by introducing the following variables:				
Dimensionless variables	$y_{CO_2} = \frac{C_{CO_2}}{C_{tot}} = C_{CO_2}\frac{\mathscr{R}T}{P}\ ;\ u^* = \frac{F_{tot}\,\tau_b}{C_{tot}\,V_b}\ ;\ z^* = \frac{z}{H}\ ;\ t^* = \frac{t}{\tau_b}$ with $\tau_b = \frac{H}{u_{in}}$			

the whole volume portion filled by gases.

In order to take into account variation of superficial gas velocity, Eq. (16) was summed with its analogue for inert N_2, considering that total molar concentration of gas phase (C_{tot}) is constant at constant pressure and temperature: the overall gaseous mole balance in that same volume (Eq. (18)) was obtained. It is worth to examine the general physicochemical meaning of Eq. (18), focusing on its right-hand side. Since temperature and pressure are constant, superficial velocity decreases because of carbonation, which subtracts gaseous moles (Reaction 1), while it grows as solid internal void fraction decreases. The latter influence can be further explained by Eqs. (7) and (4): CaO conversion causes an increase of solid volume and a decrease of pore volume within particles (because of ζ), which locally expels gases, increasing their net flow. Ultimately, Reaction 1 has two competing opposite effects on superficial velocity, a direct subtraction of gaseous moles and an indirect boost related to solid volume variation inside particles.

As far as initial conditions are concerned, CaOMAY particles were considered as completely calcined (Eq. (20)) with pure N_2 filling the whole void volume of the packed bed (Eq. (21)), flowing with an inlet superficial velocity equal to that of the reacting mixture (Eq. (22)). Danckwerts closed-closed vessel boundary conditions [1] were assumed (Eq. (23)), with the additional condition for the superficial velocity at the left boundary, derived from the overall molar inlet flow rate (Eq. (25)).

The formulation of ADPFRu(z,t) as a PDE problem (Table 3) resulted unsuitable for a numerical-integration as a unique system in MATLAB® by "pdepe" algorithm (developed for parabolic-elliptic PDE in one dimension [20]). Then, equations were algebraically manipulated so to obtain a new set of dimensionless equations (Table 4), more suitable to develop and apply ad hoc numerical-integration algorithms in MATLAB®;.

In general, PDE problems may appear in a large variety, depending on many factors (constant or variable coefficients; coordinate system; geometric classification; number of independent variables, which determines the number of dimensions; number of dependent variables, which determines the number of equations; kinds and features of boundary and initial conditions) [29]. The nonlinear, time dependent PDE problem compiled for ADPFRu(z,t) (Table 4) was defined in the dimensionless domain, and involved:

- a convection-diffusion-reaction hyperbolic-parabolic PDE (Eq. (26)) [29];
- two first-order PDEs with generative functions of z^* and t^* (Eqs. (28) and (30));
- initial conditions at $t^* = 0$ (Eqs. (31), (32), (33));
- boundary conditions on $z^* = 0,\ 1$ (Eqs. (34), (36))

Ad hoc numerical-integration algorithms were developed in MATLAB® for the ADPFRu(z,t) problem in Table 4, according to the Method of lines (MOL) [21, 29]. The basic concept in MOL involves the following steps [21]:

1. Partitioning of the solutions domain with respect to the space variable (z^* in our case), so to consider solutions only on the resulting straight lines, parallel to the time variable axis (t^* in our case);
2. Discretization, in all PDE, of partial derivatives with respect to the just partitioned space variable, so to obtain a set of Ordinary Differential Equations (ODE) in the remaining time independent variable; this ODE set approximates the original PDE problem;
3. Specification of ODE on the boundary lines of partitioned domain, by incorporating original boundary conditions into the discretization with respect to space variable (method of false boundaries);
4. Numerical solution of the initial values ODE problem, with original initial conditions specified onto the partitioned domain (finite differences methods were considered in this work to solve ODE system).

Derivatives with respect to z^* in Eq. (26) were discretized by second-order central difference approximations with a constant step-size $\Delta z^* = 1/I$ (I as the number of steps), so to obtain a three-point discretization scheme of order two:

Table 4
Dimensionless ADPFRu(z,t) and ADPFRu(const) equations, initial conditions, boundary conditions.

	ADPFRu(z,t)		ADPFRu(const)	
Dimensionless ADPFR mole balance on CO_2 in ε and ε_p	$\frac{\partial y_{CO_2}}{\partial t^*} = \frac{D_R^*}{A(X)}\frac{\partial^2 y_{CO_2}}{\partial z^{*2}} - \frac{u^*}{A(X)}\frac{\partial y_{CO_2}}{\partial z^*} - (1 - y_{CO_2})\frac{C3}{A(X)} r_{CBN}$	(26)	$\frac{\partial y_{CO_2}}{\partial t^*} = \frac{D_R^*}{A(X)}\frac{\partial^2 y_{CO_2}}{\partial z^{*2}} - \frac{u^*}{A(X)}\frac{\partial y_{CO_2}}{\partial z^*} - (1 - C5\, y_{CO_2})\frac{C3}{A(X)} r_{CBN}$	(27)
Dimensionless overall ADPFR mole balance on gas in ε and ε_p	$\frac{\partial u^*}{\partial z^*} = C4\, r_{CBN}$	(28)	$u^* = u_{in}^* = \frac{F_{in,tot}\,\tau_b}{C_{tot}\,V_b} = 1\ ,\ \forall z^*, t^*$	(29)
Dimensionless CaO dynamic conversion	$\frac{\partial X}{\partial t^*} = C1\, r_{CBN}$	(30)	$\frac{\partial X}{\partial t^*} = C1\, r_{CBN}$	(30)
	Initial conditions (IC):		Initial conditions (IC):	
Completely calcined particle	$X(\,0 \le z^* \le 1,\ t^* = 0) = 0$	(31)	$X(\,0 \le z^* \le 1,\ t^* = 0) = 0$	(31)
ε and ε_p filled by inert	$y_{CO_2}(0 \le z^* \le 1, t^* = 0) = 0$	(32)	$y_{CO_2}(0 \le z^* \le 1, t^* = 0) = 0$	(32)
Inert molar flow equal to inlet process one	$u^*(0 \le z^* \le 1, t^* = 0) = u_{in}^* = \frac{F_{in,tot}\,\tau_b}{C_{tot}\,V_b} = 1$	(33)	/	
	Boundary conditions (BC), $\forall\, t^* > 0$:		Boundary conditions (BC), $\forall\, t^* > 0$:	
Dimensionless Danckwerts closed-closed vessel boundary conditions [1]	$u_{in}^* y_{CO_2,in} = \left(u^* y_{CO_2} - D_R^* \frac{\partial y_{CO_2}}{\partial z^*}\right)\Big\vert_{z^*=0}\ ;\ \frac{\partial y_{CO_2}}{\partial z^*}\Big\vert_{z^*=1} = 0$	(34)	$u_{in}^* y_{CO_2,in} = \left(u_{in}^* y_{CO_2} - D_R^* \frac{\partial y_{CO_2}}{\partial z^*}\right)\Big\vert_{z^*=0}\ ;\ \frac{\partial y_{CO_2}}{\partial z^*}\Big\vert_{z^*=1} = 0$	(35)
Left boundary condition on u	$u^*(z^* = 0, t^*) = u_{in}^* = \frac{F_{in,tot}\,\tau_b}{C_{tot}\,V_b} = 1$	(36)	/	
Unknown functions	$X = X(z^*, t^*)\ ;\ y_{CO_2} = y_{CO_2}(z^*, t^*)\ ;\ u^* = u^*(z^*, t^*)$		$X = X(z^*, t^*)\ ;\ y_{CO_2} = y_{CO_2}(z^*, t^*)$	
Constant coefficients	$C1 = \frac{\tau_b}{n_{CaO}^0}\ ;\ C2 = (\zeta - 1)v_{CaO}\, n_{CaO}^0\ ;\ C3 = (1-\varepsilon)\frac{\tau_b}{C_{tot}}\ ;\ C4 = (1-\varepsilon)C1C2 - C3\ ;\ C5 = (\zeta - 1)v_{CaO}C_{tot}\ ;\ D_R^* = \frac{D_R \tau_b}{H^2}$			
Variable coefficients	$r_{CBN}(y_{CO_2}, X) = \frac{\sigma_{CaO}^0 n_{CaO}^0 k_s (1-X)^{2/3} C_{tot}(y_{CO_2} - y_{CO_2,eq})}{1 + \frac{n_{CaO}^0 k_s}{2D_{PL,0}\exp(-aX^b)}\delta_{CaO}^0 \sqrt[3]{1-X}\left(1 - \sqrt[3]{\frac{1-X}{1-X+X\zeta}}\right)}\ ;\ A(X) = \varepsilon + (1-\varepsilon)\,[\varepsilon_p^0 - C2\,X]$			

$$\left.\frac{\partial^2 y_{CO_2}(z^*,t^*)}{\partial z^{*2}}\right|_{z^*=z^*_{(i)}} = \frac{y^{(i-1)}_{CO_2}(t^*) - 2y^{(i)}_{CO_2}(t^*) + y^{(i+1)}_{CO_2}(t^*)}{\Delta z^{*2}} + O(\Delta z^{*2}) \quad \begin{matrix}\text{with}\\ i=0,\ldots,I\end{matrix} \tag{37}$$

$$\left.\frac{\partial y_{CO_2}(z^*,t^*)}{\partial z^*}\right|_{z^*=z^*_{(i)}} = \frac{y^{(i+1)}_{CO_2}(t^*) - y^{(i-1)}_{CO_2}(t^*)}{2\Delta z^*} + O(\Delta z^{*2}) \quad \begin{matrix}\text{with}\\ i=0,\ldots,I\end{matrix} \tag{38}$$

In Eqs. (37) and (38), the value $y^{(i)}_{CO2}(t^*)$ approximates the solution $y_{CO2}(z^*_{(i)}, t^*)$ on the line of spatial coordinate $z^* = z^*_{(i)} = i{\cdot}\Delta z^*$ belonging to the discretized domain. By replacing Eqs. (37) and (38) in Eq. (26), neglecting error terms, a set of $I+1$ dimensionless CO_2 mole balances was obtained (Eq. (39)):

$$\begin{aligned}\frac{\partial y^{(i)}_{CO_2}(t^*)}{\partial t^*} &= \left(\frac{D^*_R}{A(X^{(i)}(t^*))}\frac{1}{\Delta z^{*2}} - \frac{u^{*(i)}(t^*)}{A(X^{(i)}(t^*))}\frac{1}{2\Delta z^*}\right) y^{(i+1)}_{CO_2}(t^*)\\ &- 2\frac{D^*_R}{A(X^{(i)}(t^*))}\frac{1}{\Delta z^{*2}} y^{(i)}_{CO_2}(t^*) + \left(\frac{D^*_R}{A(X^{(i)})}\frac{1}{\Delta z^{*2}} + \frac{u^{*(i)}(t^*)}{A(X^{(i)})}\frac{1}{2\Delta z^*}\right) y^{(i-1)}_{CO_2}(t^*)\\ &- \left(1 - y^{(i)}_{CO_2}(t^*)\right)\frac{C3}{A(X^{(i)}(t^*))}\boldsymbol{r_{CBN}}\left(y^{(i)}_{CO_2}(t^*), X^{(i)}(t^*)\right) \quad \begin{matrix}\text{with}\\ i=0,\ \ldots,I\end{matrix}\end{aligned} \tag{39}$$

In Eq. (39), functions $y^{(i)}_{CO2}(t^*)$, $u^{*(i)}(t^*)$ and $X^{(i)}(t^*)$ approximate solutions $y_{CO2}(z^*_{(i)}, t^*)$, $u^*(z^*_{(i)}, t^*)$, $X^{(i)}(z^*_{(i)}, t^*)$ on the line of spatial coordinate $z^* = z^*_{(i)} = i{\cdot}\Delta z^*$ belonging to the discretized domain. When Eq. (39) is evaluated in $i = 0, I$ (i.e. the boundary points), it involves $y^{(-1)}_{CO2}(t^*)$ and $y^{(I+1)}_{CO2}(t^*)$, which lay on lines outside the discretized z^* domain: these functions were calculated by Eqs. (40) and (41), resulting from an approximation of boundary conditions (Eqs. (34) and (36)) by the central finite difference in Eq. (38) (method of false boundaries [21]).

$$y^{(-1)}_{CO_2}(t^*) = y^{(1)}_{CO_2}(t^*) + \frac{2\Delta z^*}{D^*_R}\left[u^*_{in}\, y_{CO_2,in} - u^{*(0)}(t^*)\, y^{(0)}_{CO_2}(t^*)\right] \tag{40}$$

$$y^{(I+1)}_{CO_2}(t^*) = y^{(I-1)}_{CO_2}(t^*) \tag{41}$$

Substitution of Eqs. (40) and (41) into Eq. (39) gives a set of ODE in the independent variable t^*, which must be integrated together with Eq. (30), defined on the $I+1$ lines of the space-discretized domain, all needed initial conditions being provided (Eqs. (31) and (32)). As a consequence, the resulting overall initial value problem counts $2I+2$ ODE in t^* and as many initial conditions (Eq. (42)).

$$\begin{cases}
\dfrac{\partial y^{(0)}_{CO_2}(t^*)}{\partial t^*} = \left(\dfrac{2D^*_R}{A(X^{(0)}(t^*))}\dfrac{1}{\Delta z^{*2}}\right)\left(y^{(1)}_{CO_2}(t^*) - y^{(0)}_{CO_2}(t^*)\right) + \\
\quad -\left(\dfrac{2}{A(X^{(0)})}\dfrac{1}{\Delta z^*} + \dfrac{u^{*(0)}(t^*)}{A(X^{(0)})D^*_R}\right)\left(u^{*(0)}(t^*)\, y^{(0)}_{CO_2}(t^*) - u^*_{in}\, y_{CO_2,in}\right) + \\
\quad -\left(1 - y^{(0)}_{CO_2}(t^*)\right)\dfrac{C3}{A(X^{(0)}(t^*))}\boldsymbol{r_{CBN}}\left(y^{(0)}_{CO_2}(t^*), X^{(0)}(t^*)\right) \\
\dfrac{\partial y^{(i)}_{CO_2}(t^*)}{\partial t^*} = \left(\dfrac{D^*_R}{A(X^{(i)}(t^*))}\dfrac{1}{\Delta z^{*2}} - \dfrac{u^{*(i)}(t^*)}{A(X^{(i)}(t^*))}\dfrac{1}{2\Delta z^*}\right) y^{(i+1)}_{CO_2}(t^*) + \\
\quad -\left(\dfrac{2D^*_R}{A(X^{(i)}(t^*))}\dfrac{1}{\Delta z^{*2}}\right) y^{(i)}_{CO_2}(t^*) + \left(\dfrac{D^*_R}{A(X^{(i)})}\dfrac{1}{\Delta z^{*2}} + \dfrac{u^{*(i)}(t^*)}{A(X^{(i)})}\dfrac{1}{2\Delta z^*}\right) y^{(i-1)}_{CO_2}(t^*) + \quad \text{with} \\
\quad -\left(1 - y^{(i)}_{CO_2}(t^*)\right)\dfrac{C3}{A(X^{(i)}(t^*))}\boldsymbol{r_{CBN}}\left(y^{(i)}_{CO_2}(t^*), X^{(i)}(t^*)\right) \quad i = 1,\ldots,I-1 \\
\dfrac{\partial y^{(I)}_{CO_2}(t^*)}{\partial t^*} = \left(\dfrac{2D^*_R}{A(X^{(I)}(t^*))}\dfrac{1}{\Delta z^{*2}}\right)\left(y^{(I-1)}_{CO_2}(t^*) - y^{(I)}_{CO_2}(t^*)\right) + \\
\quad -\left(1 - y^{(I)}_{CO_2}(t^*)\right)\dfrac{C3}{A(X^{(I)}(t^*))}\boldsymbol{r_{CBN}}\left(y^{(I)}_{CO_2}(t^*), X^{(I)}(t^*)\right) \\
\dfrac{\partial X^{(i)}(t^*)}{\partial t^*} = C1\,\boldsymbol{r_{CBN}}\left(y^{(i)}_{CO_2}(t^*), X^{(i)}(t^*)\right) \quad \text{with}\ i = 0,\ldots,I \\
X^{(i)}(t^* = 0) = 0 \quad \text{with}\ i = 0,\ldots,I \\
y^{(i)}_{CO_2}(t^* = 0) = 0
\end{cases} \tag{42}$$

Whatever the method chosen to numerically integrate the ODE system in Eq. (42), one must know $u^{*(i)}(t^*)$, for which there is not an equation with a first-order derivative with respect to t^* to be included in that integration. This issue was worked out by discretizing Eq. (28): its first order derivative with respect to z^* was approximated with the forward finite difference defined in Eq. (43), so to obtain the algebraic problem in Eq. (44) (explicit Euler method [21]).

$$\left.\frac{\partial u^*(z^*,t^*)}{\partial z^*}\right|_{z^*=z^*_{(i)}} = \frac{u^{*(i+1)}(t^*) - u^{*(i)}(t^*)}{\Delta z^*} + O(\Delta z^*) \quad \begin{matrix}\text{with}\\ i=0,\ldots,I\end{matrix} \tag{43}$$

$$\begin{cases} u^{*(i+1)}(t^*) = u^{*(i)}(t^*) + \Delta z^*\ C4\ \boldsymbol{r_{CBN}}\left(y^{(i)}_{CO_2}(t^*), X^{(i)}(t^*)\right) \\ u^{*(0)}(t^*=0) = u^*_{in} \end{cases} \quad \begin{matrix}\text{with}\\ i=0,\ldots,I-1\end{matrix} \tag{44}$$

The problem in Eq. (44) must be solved at the beginning of each step of the chosen integration procedure on independent variable t^* for the overall ODE system (Eq. (42)), so to provide needed $u^{*(i)}(t^*)$ values at that step.

In principle, numerical integration with respect to t^* could be carried out by explicit or implicit Euler methods, or any of the higher-order finite differences methods for initial values ODE problems [21, 30].

Stability constraints do exist in the application of explicit methods to compute numerical approximations of solutions of initial values ODE problems [30]: the need to lower Δz^*, in order to achieve a better accuracy on the space variable, demands to decrease at the same time the step-size $\Delta t^* = t^*_{fin}/J$ adopted to discretize t^* (with J as the number of steps).

When the explicit Euler method [21] was chosen for the solution of the ODE system in Eq. (42), relevant numerical instabilities appeared in its numerical-integration by MATLAB®. In fact, assuming $t_{fin} = 1$ h, the dimensionless time step-size Δt^* had to be reduced very drastically (minimum J in the order of 10^5) to fulfil the standard stability criterion of Courant-Friederich-Levy specified for our case of study (Eq. (45)) [31, 32, 33], even with a rough discretization on z^* (e.g. $I = 10$, 30). In other words, with explicit Euler computation procedure applied to our ODE system, efforts to minimize truncation errors require a great number of calculations and therefore long computational time (in the order of several hours with an ordinary up-to-date computer), furthermore involving at the same time the risk of an increase of roundoff error. As a consequence, more refined numerical-integration methods were considered, so to get accurate solution approximations in a reasonable time and with a fair computational burden.

$$\frac{\Delta t^*}{\Delta z^{*2}} \cdot max\left|\frac{D^*_R}{A(X)}\right| \leq \frac{1}{2} \tag{45}$$

Implicit methods can circumvent stability issues; anyway, they generally bring in more onerous algebraic elaborations [30], a problem even more emphasized by the complexity of the ODE system for the investigated case of study (Eq. (42)). Consequently, other explicit integrators, more elaborate than explicit Euler method, were considered among ODE solvers provided by MATLAB® [34]. All these MATLAB® functions automatically determine the step-size required to obtain a prescribed accuracy. With regard to simulations of the case of study discussed in Section 4, the "ode23tb" solver was used, which compares trapezoidal rule with backward differentiation method, to estimate the suitable Δt^*.

The just described procedure is schematized by the flowchart in Fig. 2.

3.2. Development of ADPFRu(const) numerical-integration

Table 3 summarizes the whole set of equations, initial and boundary conditions for ADPFRu(const) option.

It was obtained by imposing the simplifying hypothesis of constant superficial velocity in ADPFRu(z,t), here set identically equal to its inlet value (Eq. (19)); Eq. (17) resulted as the mole balance for CO_2, a direct application of Eq. (3) to the current case of study.

Initial and boundary conditions were the same used for ADPFRu(z,t), with the only exception of those about superficial velocity, not needed in this case.

Even though the hypothesis of constant superficial velocity would have allowed the use of "pdepe" in MATLAB® (as done in [6, 7]), the same ad hoc numerical-integration developed for ADPFRu(z,t) was applied to ADPFRu(const), in order to fairly compare results from the two options. Equations in Table 3 were rearranged as shown in Table 4, so to be discretized as explained in Section 3.1, considering $u^{*(i)}(t^*)$ identically equal to its initial value (Eq. (29)). As a consequence, the related further numerical integration by the explicit Euler method (Eqs. (43) and (44)) was not required in this case.

The flowchart describing the ADPFRu(const) option can be obtained by modifications in Fig. 2, substituting equations with those related to ADPFRu(const) option (correspondingly reported in Tables 3 and 4) and omitting all steps concerning calculations of variable u^*.

4. Results and discussion

4.1. Physicochemical characterization

XRD spectrum for CaOMAY confirmed the presence of main desired crystalline phases, mayenite ($Ca_{12}Al_{14}O_{33}$) and CaO (Fig. 3 a), identified by comparison with PDF (Powder Diffraction Files) from the database of the ICDD (International Centre of Diffraction Data). The composition detected by XRD corroborates the usage of PGM to interpret CAOMAY behaviour. Average crystallite dimensions calculated by Scherrer equation [23, 25, 26] were respectively 30.6 nm and 33.1 nm. Measured particle density and void fraction of CaOMAY are in Table 5.

4.2. TGA data fitting by PGM

The experimental value of Γ for CaOMAY, obtained from the 7 h TGA experiment, was 0.24 g_{CO2} per g of calcined material, assumed to correspond to 100 % CaO conversion (X). Fig. 3 b shows experimental values of X from TGA test, compared with the corresponding output of PGM set with constants and parameters in Table 5 and with $a = 22.7$, $b = 0.35$, $\delta^0_{CaO} = 69.5$ nm (2.1 times the Scherrer average crystallite dimension): these values gave a very good agreement between CaOMAY experimental behaviour and simulations by the PGM.

4.3. ADPFR simulations: results and their physicochemical evaluation

The values of parameters a, b and δ^0_{CaO} found in Section 4.2 were assumed for simulations by means of ADPFRu(z,t) and ADPFRu(const), presented in Section 3. Since the simulated reactor is the same studied in [6], the same values for packed void fraction ($\varepsilon = 0.5$) and axial dispersion coefficient ($D_R = 10^{-5}$ m^2 s^{-1}) were used in this study. They completed the set of parameters (Table 5) utilized in all simulations; this set can be considered as representative of the studied system thanks to comparisons between related numerical outputs and experimental data, already performed in this work by TGA/PGM fitting or elsewhere for packed bed reactor features [6].

The comparison between the performances of both ADPFR numerical integrations was carried out by simulating the case of study described in Section 2.1, assuming different CO_2 concentrations in the inlet stream (mole fraction $y_{CO2,in} = 0.15$; 0.45; 0.70; 0.90).

To help comparing outputs of different simulations one to each other, as well as evaluating their coherence with actual physicochemical phenomena, numerical results were expressed in terms of outlet CO_2 molar fraction ($y_{CO2,out}$), relative deviation of inert flow rate ($\Delta F_{N2,out}(t)$, Eq.

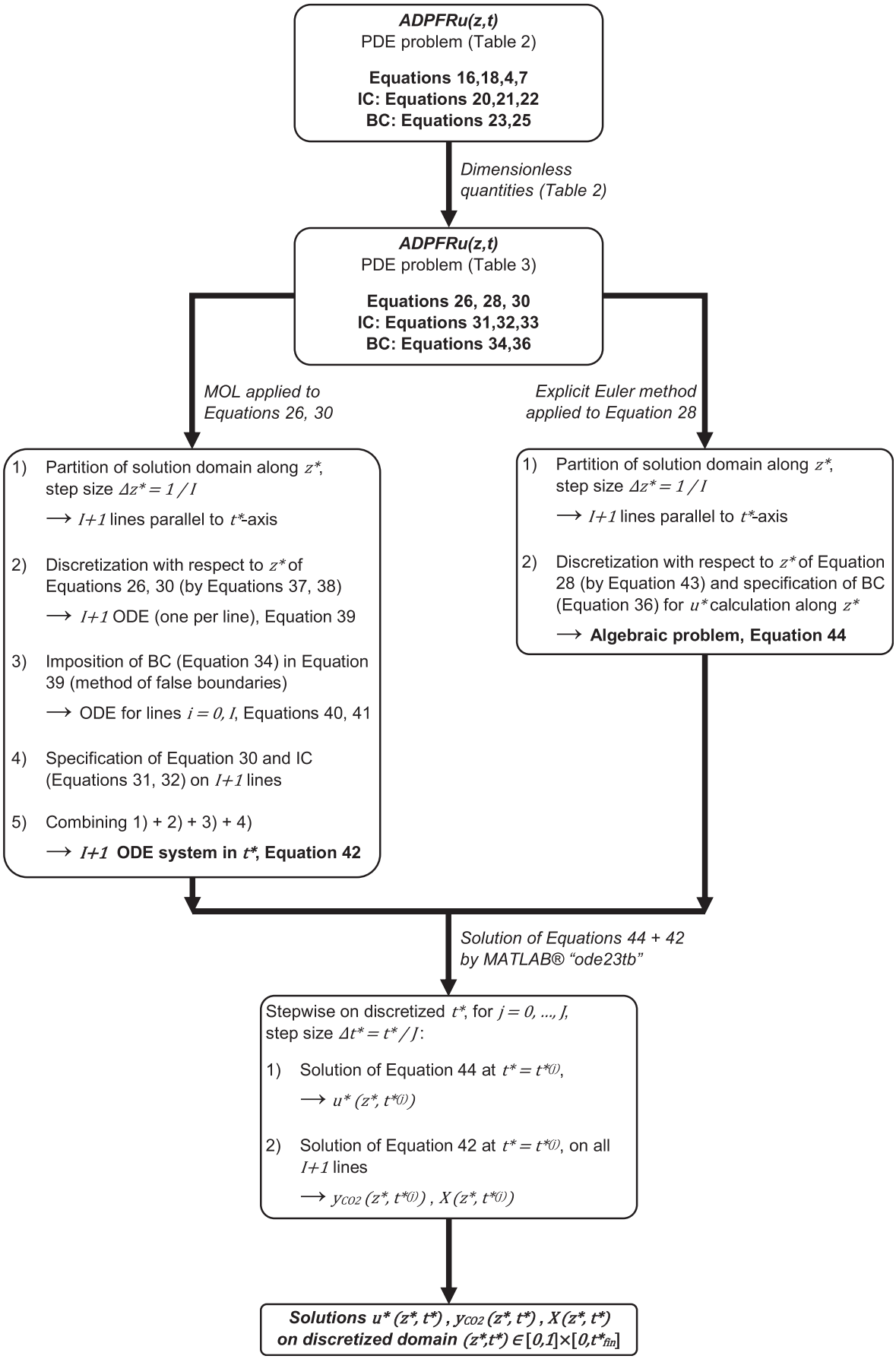

Fig. 2. Flowchart describing development and solution of ADPFR model for the case of study, according to ADPFRu(z,t) option.

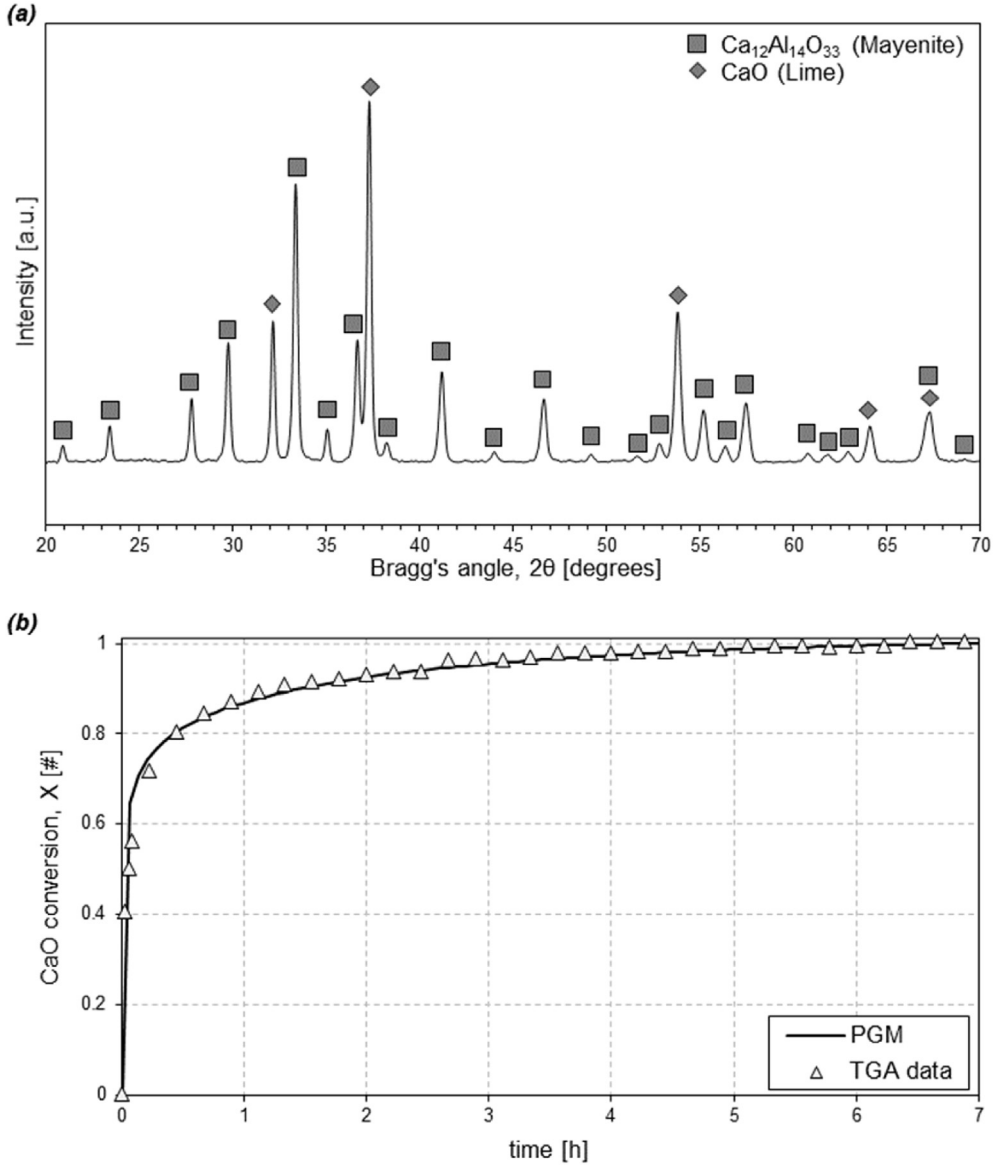

Fig. 3. Characterization of CaOMAY: (a) XRD spectrum with detected crystalline phases ($Ca_{12}Al_{14}O_{33}$ PDF: 00-009-0413; CaO PDF: 00-037-1497); (b) Experimental data of CO_2-capture TGA test and corresponding PGM simulation of CaO conversion (X) as a function of time ($a = 22.7$, $b = 0.35$, $\delta^0_{CaO} = 69.5$ nm).

(47)) and cumulative CO_2 mole balance ($\Delta N_{CO2}(t)$, Eq. (53)). $\Delta F_{N2,out}(t)$ represents the percentage deviation of N_2 outlet flow rate with respect to the corresponding inlet value. $\Delta N_{CO2}(t)$ is the percentage deviation between total moles of CO_2 fed to the reactor until a given time instant t, ($N_{CO2,in}(t)$, Eq. (49)) and the sum of CO_2 moles that have left the reactor until t ($N_{CO2,out}(t)$, Eq. (50)), have been captured by the sorbent until t ($NC_{O2,capt}(t)$, Eq. (51)) and are in the reactor void volume at the very same instant t ($N_{CO2,Vb}(t)$, Eq. (52)); theoretical evaluations of the actual physicochemical process suggest that $\Delta N_{CO2}(t)$ should be zero in real cases.

$$F_{N_2}(z,t) = u^*(z,t)\frac{V_b\, C_{tot}}{\tau_b} - SC_{tot}\left[-D_R\frac{\partial y_{CO_2}(z,t)}{\partial z} + u^*(z,t)\frac{H}{\tau_b}y_{CO_2}(z,t)\right] \tag{46}$$

$$\Delta F_{N_2,out}(t) = \frac{F_{N_2}(z^*=1,t) - F_{N_2,in}}{F_{N_2,in}}\ 100 \tag{47}$$

$$F_{CO_2}(z,t) = SC_{tot}\left[-D_R\frac{\partial y_{CO_2}(z,t)}{\partial z} + u^*(z,t)\frac{H}{\tau_b}y_{CO_2}(z,t)\right] \tag{48}$$

$$N_{CO_2,in}(t) = \int_0^t F_{CO_2,in}(t)dt = F_{CO_2,in}\ t \tag{49}$$

$$N_{CO_2,out}(t) = \int_0^t F_{CO_2}(z^*=1,t)dt \tag{50}$$

$$N_{CO_2,capt}(t) = \frac{w^0_{CaO}\, m^0_b}{M_{CaO}\, H}\int_0^z X(z,t)dz \tag{51}$$

$$N_{CO_2,V_b}(t) = SC_{tot}\int_0^z \left[\varepsilon_b\, y_{CO_2}(z,t) + (1-\varepsilon_b)\ \varepsilon_p(z,t)\ y_{CO_2}(z,t)\right]dz \tag{52}$$

Table 5
Constant parameters assumed for PGM and ADPFR simulations.

Process conditions and physical parameters:		
	PGM	**ADPFR**
Temperature, T [°C]	650	650
Pressure, P [atm]	1	1
CO_2 molar fraction in the gaseous bulk, $y_{CO2,bulk}$ [mol/mol]	0.15	/
CO_2 molar fraction in the inlet gas, $y_{CO2,in}$ [mol/mol]	/	0.15; 0.45; 0.75; 0.90
Total inlet flow rate, $F_{tot,in}$ [Nml min^{-1}]	/	20
Reactor diameter [m]	/	$7 \cdot 10^{-3}$
Average particle diameter, d_p [μm]	72	112.5
Sorption capacity, Γ [g_{CO2} $g^{-1}_{CaOMAY\text{-}calcined}$]^	0.24	0.24
Initial particle density, ρ^0_p [kg m^{-3}]^^	1693	1693
Initial particle void fraction, ε^0_p [#]^^^	0.40	0.40
Model parameters:		
	PGM	**ADPFR**
CBN rate constant, k_s [m^4 $kmol^{-1}$ s^{-1}] [28]	$5.95 \cdot 10^{-7}$	$5.95 \cdot 10^{-7}$
α [#] [35, 36]	1.65	1.65
a [#]	22.7	22.7
b [#]	0.35	0.35
Initial CaO grain diameter, δ^0_{CaO} [nm]	69.5	69.5
Axial dispersion coefficient, D_R [m^2 s^{-1}]	/	10^{-5}
Packed bed void fraction, ε [#]	/	0.5

^ experimentally determined by TGA measurement.
^^ experimentally determined by GEOPYC 1360.
^^^ experimentally determined by ACCUPYC 1330 pycnometer.

$$\Delta N_{CO_2}(t) = \frac{N_{CO_2,in}(t) - \left[N_{CO_2,out}(t) + N_{CO_2,capt}(t) + N_{CO_2,V_b}(t)\right]}{N_{CO_2,in}(t)} \; 100 \qquad (53)$$

Fig. 4 shows the main outputs of simulations from the two ADPFR numerical integrations, with $y_{CO2,in} = 0.15$ and process duration of 1800 s. Main differences between the two models appeared clearly. In fact, the ADPFRu(z,t) integration was capable of computing superficial velocity as a function of z and t, producing a quantitative trend in agreement with the expected progression of CO_2 capture phenomena (Fig. 4 a): where and when Reaction 1 occurred preferentially (reduction of $y_{CO2}(z,t)$ and increase of CaO conversion $X(z,t)$), a corresponding decrease of the dimensionless superficial velocity $u^*(z,t)$ was evident. On the other hand, the ADPFRu(const) integration could not provide a variable superficial velocity, even though it calculated similar trends for $y_{CO2}(z,t)$ and $X(z,t)$ (Fig. 4 b). It is worth to make further comment on superficial velocity surface in Fig. 4: with regard to the discussion about Eq. (18) made in Section 3.1, the shape of this surface clearly showed that the prevailing effect of carbonation (Reaction 1) on u^* was the subtraction of CO_2 from the gas phase.

Fig. 5 represents values of $y_{CO2,out}$ as a function of time, resulting from simulations with both ADPFR numerical options. For each $y_{CO2,in}$, both models agreed in predicting: (i) the qualitative shape of $y_{CO2,out}$ curves; (ii) the beginning of packed bed breakthrough (the moment at which CO_2 molar fraction breaks away from the initial plateau equal to 0.0096, the equilibrium value at 1 atm and 650 °C for Reaction 1 [37]); (iii) the post-breakthrough plateau, which tends to the corresponding value of $y_{CO2,in}$. The only discrepancies between $y_{CO2,out}$ from ADPFRu(z,t) and ADPFRu(const) occurred in the shape of the breakthrough curve: the higher $y_{CO2,in}$, the steeper the breakthrough trend for ADPFRu(z,t) in comparison to that predicted by ADPFRu(const); the lower $y_{CO2,in}$, the closer the breakthrough curves from the two options.

For a given sorbent material, Di Giuliano et al. [7] and Aloisi et al. [6] demonstrated that carbonation kinetic parameters from PGM/TGA fitting allow an ADPFR dynamic model to faithfully predict the CO_2 capture performance carried out by a packed bed of that material during SESMR, with flowing reactants diluted in inert gas and then under the assumption of constant superficial velocity in numerical-integration. The same PGM/TGA fitting procedure was used in this work to provide specific parameters to simulate CaOMAY behaviour with both ADPFRu(z,t) and ADPFRu(const) options. Based on this, the high similarity of $y_{CO2,out}$ curves, for a given $y_{CO2,in}$, constituted a validation of ADPFRu(z,t) option, at least for the most diluted cases (Fig. 5, $y_{CO2,in} = 0.15, 0.45$). In addition, in the light of points (i), (ii), (iii) listed just above, for each given $y_{CO2,in}$ the two $y_{CO2,out}$ curves from ADPFRu(z,t) and ADPFRu(const) resulted similar in many respects, which moreover corresponded to correct physicochemical conclusions: $y_{CO2,out}$ before breakthrough was extremely close to the CO_2 equilibrium molar fraction at 1 atm and 650 °C (according to [37]), i.e. both ADPFRu(z,t) and ADPFRu(const) options predicted that the completely calcined packed bed was fully active and made carbonation approach equilibrium, a first reasonable conclusion; $y_{CO2,out}$ after breakthrough resulted very close to $y_{CO2,in}$, i.e. the model predicted, again with both ADPFRu(z,t) and ADPFRu(const) options, that the saturated packed bed left the flowing gas unchanged, a second reasonable conclusion.

Fig. 6 shows the most relevant difference in computations between ADPFRu(z,t) and ADPFRu(const), linked to the ability of the former to compute superficial velocity as a function of z and t, differently from the latter, exploiting a simplified numerical treatment. In the ADPFRu(const) integration, because of the assumption of constant superficial gas velocity, the decrease of CO_2 concentration due to Reaction 1 ($y_{CO2,in}(z,t)$) was unrealistically balanced by an increase of N_2 molar flow rate (Fig. 6 b and d). On the other hand, ADPFRu(z,t) option allowed to keep outlet inert flow rate close to more conceivable values as long as carbonation occurred (Fig. 6 a and c). In fact, for a given $y_{CO2,in}$, absolute values of $\Delta F_{N2,out}(t)$ were definitely greater in simulations with ADPFRu(const) (Fig. 6 b, d, f) than in those with ADPFRu(z,t) (Fig. 6 a, c, e), with a difference of at least one order of magnitude at any given time. As we get from Fig. 6, as long as reactive gaseous species CO_2 is converted into $CaCO_3$, the more concentrated the inlet CO_2 stream, the greater $\Delta F_{N2,out}(t)$. From the physicochemical point of view, this systematic and abnormally high increase of N_2 flow rate during carbonation, imposed by ADPFRu(const) option, is definitely less reasonable than corresponding predictions of ADPFRu(z,t). This highlights an inherent vice in the ADPFRu(const) option, due to the hypothesis of constant superficial velocity: a fictitious variation of inert moles is forced in contradiction with principle of mass conservation, in order to fulfil just that very same hypothesis.

The ability of ADPFRu(z,t) in computing superficial velocity as a function of z and t determined better performances than ADPFRu(const) also in terms of $\Delta N_{CO2}(t)$, as shown in Fig. 7. ADPFRu(z,t) gave values for $\Delta N_{CO2}(t)$ within the range ±3 % (Fig. 7 a, c, e), systematically smaller than those obtained by ADPFRu(const), as long as carbonation occurs and $y_{CO2,in}$ being equal. During CO_2 conversion, the ADPFRu(z,t) option provided solutions decidedly closer to the condition $\Delta N_{CO2}(t) = 0$ (a direct consequence from principle of mass conservation) with respect to those from ADPFRu(const), therefore the former were in better agreement with the expected physicochemical phenomena. As far as ADPFRu(const) results for $\Delta N_{CO2}(t)$ are concerned, the trend with respect to $y_{CO2,in}$ was inverse than what observed for $\Delta F_{N2,out}(t)$: the lower $y_{CO2,in}$ the higher $\Delta N_{CO2}(t)$.

Similarities in $y_{CO2,out}$ numerical predictions from the two options suggest that ADPFRu(const), thanks to its lower numerical complexity, may be a sensible choice in the case of diluted reactants or when $y_{CO2,out}$ qualitative evolution is the only information of interest. However, mass conservation biases identified for the ADPFRu(const) option, thanks to evaluations on $\Delta F_{N2,out}(t)$ and $\Delta N_{CO2}(t)$, highlighted that inferences from its solutions might lead to very conspicuous quantitative errors in terms of moles balances, beyond possible numerical roundoff errors or approximations, albeit in the face of reasonable predictions of $y_{CO2,out}$; in this regard, ADPFRu(z,t) appeared by far as the most reliable option, with the most coherent moles balances, in better agreement with expected trends of the actual physicochemical process. This constitutes a good point in terms of validation, to the benefit of ADPFRu(z,t) option.

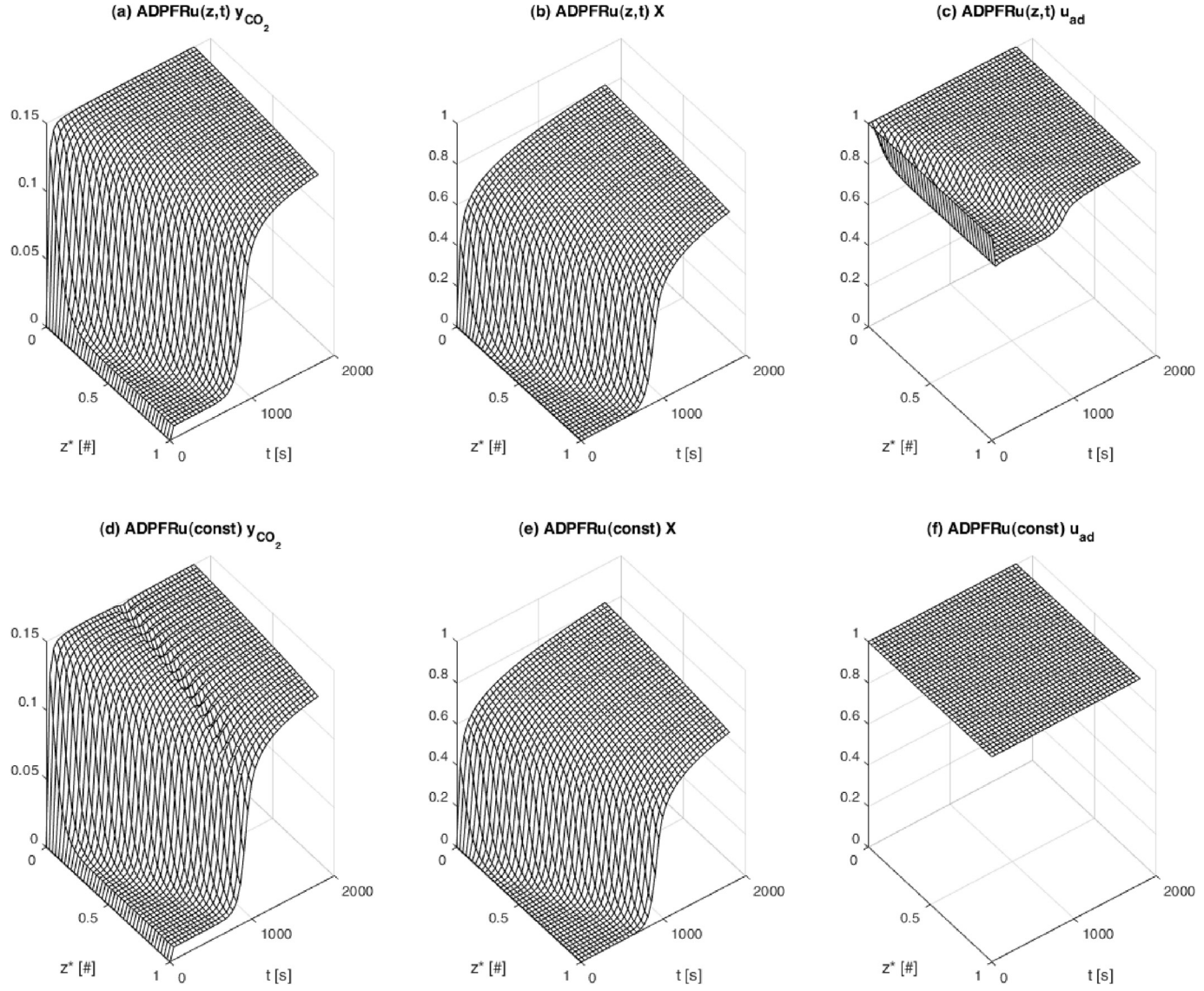

Fig. 4. Results from simulations of the case of study (with inlet CO_2 molar fraction $y_{CO2,in} = 0.15$ and process duration of 1800 s) by both integration options: (a) ADPFRu(z,t) CO_2 molar fraction; (b) ADPFRu(z,t) CaO conversion; (c) ADPFRu(z,t) dimensionless superficial gas velocity; (d) ADPFRu(const) CO_2 molar fraction; (e) ADPFRu(const) CaO conversion; (f) ADPFRu(const) dimensionless superficial gas velocity.

5. Conclusions

Numerical integration of ADPFR dynamic models with variable superficial velocity is still a little explored issue in chemical reactors engineering. This work presented a method which aims to make a contribution to fill this gap.

The case of study of CO_2 capture from a CO_2/N_2 stream on a solid sorbent, by means of a CaO-mayenite packed bed reactor, was modelled as an ADPFR with two approaches, the former involving variation of the overall superficial gas velocity as a function of time and reactor length (named ADPFRu(z,t)), the latter assuming the often applied hypothesis to neglect any change in the volumetric flow rate (named ADPFRu(const)).

A numerical-integration approach was proposed, based on the MOL associated with the MATLAB® ODE solver "ode23tb" to guarantee numerical stability, and with the explicit Euler method to compute superficial velocity function at a given time in the case of ADPFRu(z,t). This approach was successful in approximating solutions of both ADPFRu(z,t) and ADPFRu(const) sets of partial differential equations; this represents a relevant achievement, considering the little deepening dedicated so far to ADPFR modelling with variable superficial velocity. Moreover, it could be further extended to multiple reaction systems, also thanks to the choice of concentrations in the gas phase as dependent functional variables.

Functions of superficial gas velocity in the ADPFRu(z,t) case (numerical-integration by MOL, "ode23tb" and explicit Euler method), were in agreement with expected trends of actual reactive phenomena of the case of study.

A comparative analysis between results from ADPFRu(z,t) and ADPFRu(const) was focused on predictions of outlet CO_2 molar fraction, outlet N_2 molar flow rate and cumulative CO_2 mole balance, for the whole process duration and with variation of inlet CO_2 concentration; some distortions arose from the simplifying hypothesis of constant superficial gas velocity:

- As the inlet CO_2 concentration increased, more and more different predictions were obtained on the shape of CO_2 concentration as a

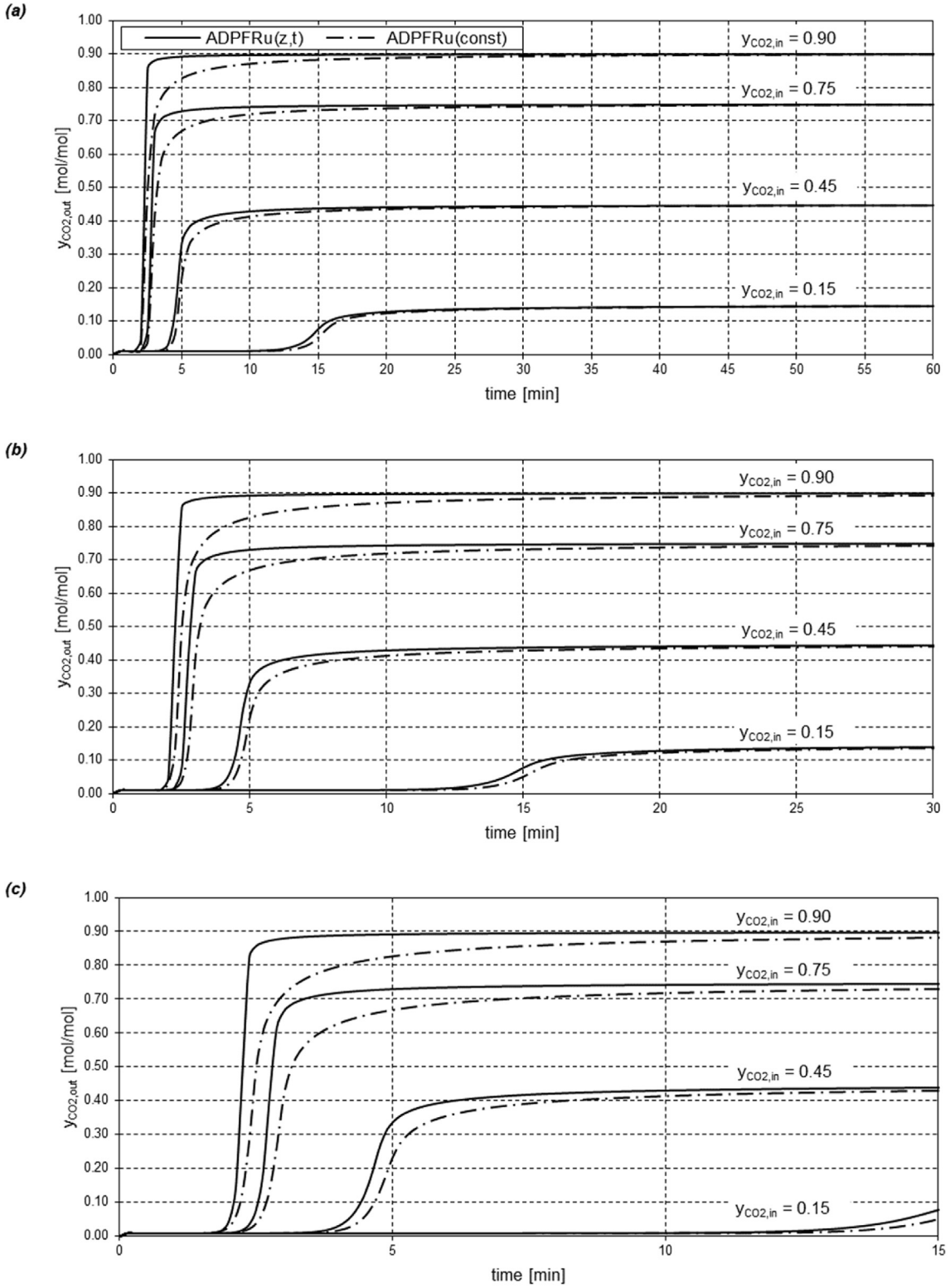

Fig. 5. ADPFRu(z,t) and ADPFRu(const) simulations of outlet CO_2 molar fraction ($y_{CO2,out}$) as a function of time, for different values of inlet CO_2 molar fraction ($y_{CO2,in}$ = 0.15; 0.45; 0.70; 0.90): (a) whole simulated process duration (60 min); (b) magnification of the first 30 min; (c) magnification of the first 15 min. Legend in (a) is valid for all pictures.

function of time in outlet stream; this corroborates the introductive statement about suitability of simplified ADPFR models only for tubular reactors fed with diluted reactants.

- As long as CO_2 (reactive species) was captured, ADPFRu(const) determined a relevant fictitious increase of inert N_2 flow rate (which cannot actually occur), in order to keep the overall flow rate equal to its inlet value; this may involve wrong estimations on process variables, if pressure drops in the packed bed would be considered, for instance. On the other hand, ADPFRu(z,t) appeared as a more reliable

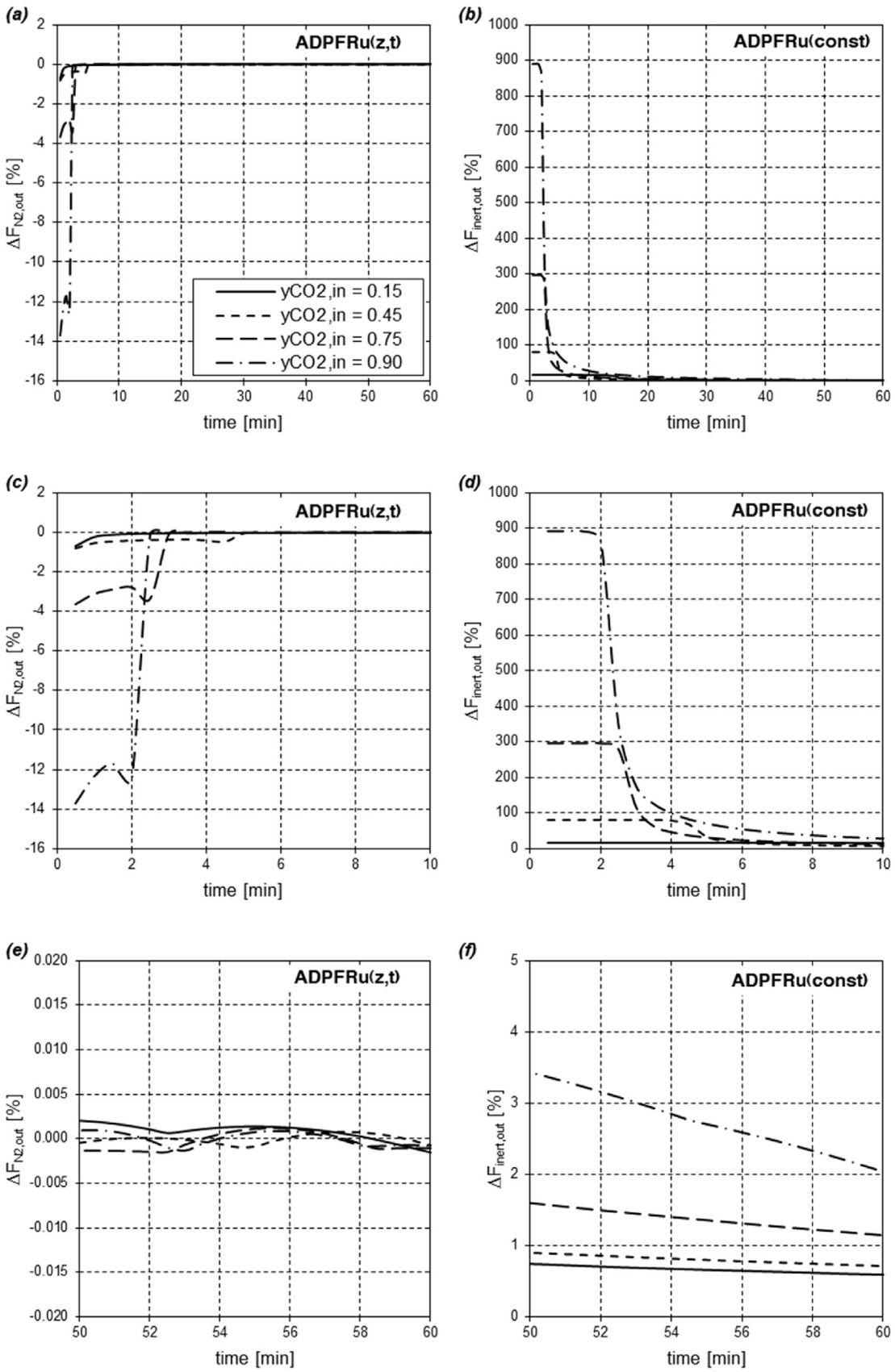

Fig. 6. Simulations of outlet N_2 flow rate as a function of time, expressed as $\Delta F_{N2,out}(t)$, for different values of inlet CO_2 molar fraction ($y_{CO2,in} = 0.15; 0.45; 0.70; 0.90$): (a) ADPFRu(z,t) results; (b) ADPFRu(const) results; (c) magnification of the first 10 min from ADPFRu(z,t) results; (d) magnification of the first 10 min from ADPFRu(const) results; (e) magnification of the last 10 min from ADPFRu(z,t) results; (f) magnification of the last 10 min from ADPFRu(const) results. Legend in (a) is valid for all pictures.

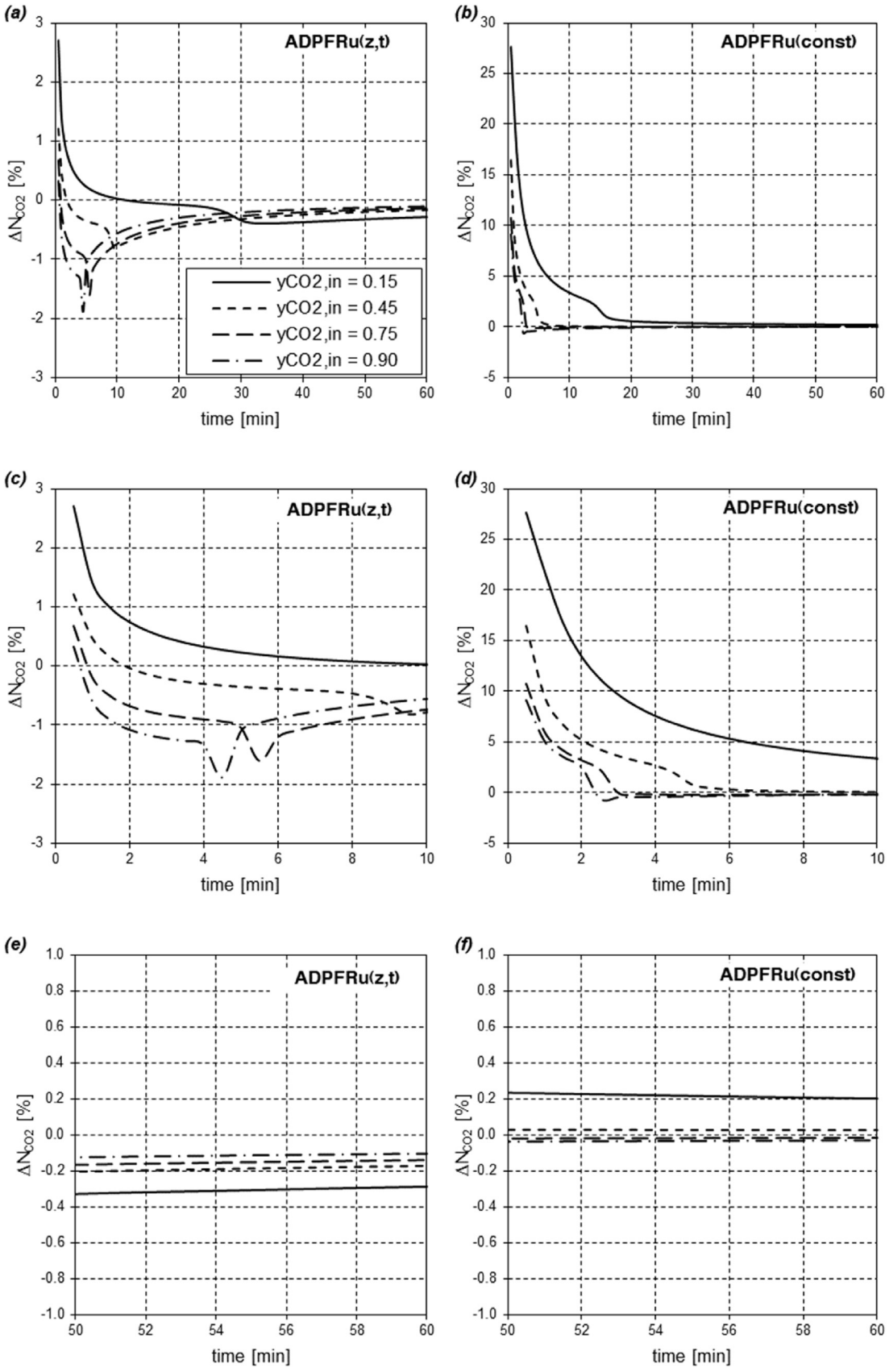

Fig. 7. Cumulative CO_2 mole balance as a function of time, expressed as $\Delta N_{CO2}(t)$, for different values of inlet CO_2 molar fraction ($y_{CO2,in} = 0.15; 0.45; 0.70; 0.90$) (a) ADPFRu(z,t) results; (b) ADPFRu(const) results; (c) magnification of the first 10 min from ADPFRu(z,t) results; (d) magnification of the first 10 min from ADPFRu(const) results; (e) magnification of the last 10 min from ADPFRu(z,t) results; (f) magnification of the last 10 min from ADPFRu(const) results. Legend in (a) is valid for all pictures.

tool, in terms of compliance with the principle of mass conservation, as it keeps outlet N_2 flow rate close to its inlet value.
- Additionally, ADPFRu(z,t) was more reliable than ADPFRu(const) on predicting the CO_2 cumulative moles balance.

All this considered, the simplifying assumption of uniform superficial velocity in ADPFR modelling should be carefully evaluated. It brings in a less sophisticated mathematical model, so that it is reasonable to use when allowed by process features and according to the output information needed. Otherwise, the combination of MOL with a proper ODE integration method and the explicit Euler method was proved to be a valuable option to solve numerically complex PDE systems, associated with convection-diffusion-reaction phenomena which make the hypothesis of constant superficial velocity an unrealistic approximation.

Declarations

Author contribution statement

Andrea Di Giuliano, Enza Pellegrino: Conceived and designed the experiments; Performed the experiments; Analyzed and interpreted the data; Contributed reagents, materials, analysis tools or data; Wrote the paper.

Funding statement

This work was supported by the European Union's Seventh Framework Program ASCENT grant agreement n° 608512.

Competing interest statement

The authors declare no conflict of interest.

Additional information

No additional information is available for this paper.

Acknowledgements

Authors thank Fabiola Ferrante and Giampaolo Antonelli for their technical support to experimental activities, as well as Prof. P. U. Foscolo for his inspiring advice.

References

[1] H.S. Fogler, Elements of Chemical Reaction Engineering, 2005.
[2] J.M. Smith, Chemical Engineering Kinetics, third ed., McGraw-Hill, New York, n.d.
[3] O. Levenspiel, Chemical Reaction Engineering, Wiley, 1972.
[4] F. Shiraishi, Highly accurate solution of the axial dispersion model expressed in S-system canonical form by Taylor series method, Chem. Eng. J. 83 (2001) 175–183.
[5] J. Roininen, V. Alopaeus, The moment method for one-dimensional dynamic reactor models with axial dispersion, Comput. Chem. Eng. 35 (2011) 423–433.
[6] I. Aloisi, A. Di Giuliano, A. Di Carlo, P.U. Foscolo, C. Courson, K. Gallucci, Sorption enhanced catalytic Steam Methane Reforming: experimental data and simulations describing the behaviour of bi-functional particles, Chem. Eng. J. (2016).
[7] A. Di Giuliano, K. Gallucci, F. Giancaterino, C. Courson, P.U. Foscolo, Multicycle sorption enhanced steam methane reforming with different sorbent regeneration conditions: experimental and modelling study, Chem. Eng. J. (2018).
[8] B. Giojelli, C. Verdier, J.Y. Hihn, J.F. Béteau, A. Rozzi, Identification of axial dispersion coefficients by model method in gas/liquid/solid fluidised beds, Chem. Eng. Process. Process Intensif. 40 (2001) 159–166.
[9] W. Yang, J. Wang, L. Zhou, Y. Jin, Gas–liquid mass transfer behavior in three-phase CFB reactors, Chem. Eng. Sci. 54 (1999) 5523–5528.
[10] T. Zhang, B. Zhao, J. Wang, Mathematical models for macro-scale mass transfer in airlift loop reactors, Chem. Eng. J. 119 (2006) 19–26.
[11] H.T. Bi, N. Ellis, I.A. Abba, J.R. Grace, A state-of-the-art review of gas-solid turbulent fluidization, Chem. Eng. Sci. 55 (2000) 4789–4825.
[12] M.L. Thompson, H. Bi, J.R. Grace, A generalized bubbling/turbulent fluidized-bed reactor model, Chem. Eng. Sci. 54 (1999) 2175–2185.
[13] I.A. Abba, J.R. Grace, H. Bi, M.L. Thompson, Spanning the flow regimes: generic fluidized-bed reactor model, AIChE J. 49 (2003) 1838–1848.
[14] J. Chaouki, A. Gonzalez, C. Guy, D. Klvana, Two-phase model for a catalytic turbulent fluidized-bed reactor: application to ethylene synthesis, Chem. Eng. Sci. 54 (1999) 2039–2045.
[15] M. Foka, J. Chaouki, C. Guy, D. Klvana, Gas phase hydrodynamics of a gas-solid turbulent fluidized bed reactor, Chem. Eng. Sci. 51 (1996) 713–723.
[16] I.A. Abba, J.R. Grace, H.T. Bi, Variable-gas-density fluidized bed reactor model for catalytic processes, Chem. Eng. Sci. 57 (2002) 4797–4807.
[17] G.F. Froment, Fixed bed catalytic reactors — current design status, Ind. Eng. Chem. 59 (1967) 18–27.
[18] S. Stendardo, P.U. Foscolo, Carbon dioxide capture with dolomite: a model for gas–solid reaction within the grains of a particulate sorbent, Chem. Eng. Sci. 64 (2009) 2343–2352.
[19] I. Aloisi, N. Jand, S. Stendardo, P.U. Foscolo, Hydrogen by sorption enhanced methane reforming: a grain model to study the behavior of bi-functional sorbent-catalyst particles, Chem. Eng. Sci. 149 (2016) 22–34.
[20] MathWorks, MATLAB pdepe - MathWorks, n.d. https://it.mathworks.com/help/matlab/ref/pdepe.html?s_tid=doc_ta. (Accessed 15 December 2018).
[21] M.E. Davis, Numerical Methods and Modeling for Chemical Engineers, Courier Corporation, 2013.
[22] A. Di Giuliano, K. Gallucci, P.U. Foscolo, C. Courson, Effect of Ni precursor salts on Ni-mayenite catalysts for steam methane reforming and on Ni-CaO-mayenite materials for sorption enhanced steam methane reforming, Int. J. Hydrogen Energy 44 (2019) 6461–6480.
[23] A. Di Giuliano, J. Girr, R. Massacesi, K. Gallucci, C. Courson, Sorption enhanced steam methane reforming by Ni–CaO materials supported on mayenite, Int. J. Hydrogen Energy 42 (2017) 13661–13680.
[24] A. Di Giuliano, F. Giancaterino, K. Gallucci, P.U. Foscolo, C. Courson, Catalytic and sorbent materials based on mayenite for sorption enhanced steam methane reforming with different packed-bed configurations, Int. J. Hydrogen Energy 43 (2018) 21279–21289.
[25] A. Monshi, Modified scherrer equation to estimate more accurately nano-crystallite size using XRD, World J. Nano Sci. Eng. 02 (2012) 154–160.
[26] J.I. Langford, A.J.C. Wilson, Scherrer after sixty years: a survey and some new results in the determination of crystallite size, J. Appl. Crystallogr. 11 (1978) 102–113.
[27] A. Di Giuliano, F. Giancaterino, C. Courson, P.U. Foscolo, K. Gallucci, Development of a Ni-CaO-mayenite combined sorbent-catalyst material for multicycle sorption enhanced steam methane reforming, Fuel 234 (2018) 687–699.
[28] S.K. Bhatia, D.D. Perlmutter, Effect of the product layer on the kinetics of the CO2-lime reaction, AIChE J. 29 (1983) 79–86.
[29] S. Hamdi, W. Schiesser, G. Griffiths, Method of lines, Scholarpedia 2 (2007) 2859.
[30] E. Pellegrino, E. Santi, Calcolo Numerico : Metodi Ed Applicazioni Usando MATLAB, Aracne, 2014.
[31] A. Jinasena, G.-O. Kaasa, R. Sharma, Use of Orthogonal Collocation Method for a Dynamic Model of the Flow in a Prismatic Open Channel: for Estimation Purposes, 2017, pp. 90–96.
[32] A. Bollermann, G. Chen, A. Kurganov, S. Noelle, A well-balanced reconstruction of wet/dry fronts for the shallow water equations, J. Sci. Comput. 56 (2013) 267–290.
[33] A. Kurganov, G. Petrova, A Second-Order Well-Balanced Positivity Preserving Central-upwind Scheme for the Saint-Venant System *, International Press, 2007. https://projecteuclid.org/download/pdf_1/euclid.cms/1175797625. (Accessed 4 December 2018).
[34] MathWorks, Choose an ODE Solver - MATLAB & Simulink - MathWorks Italia, n.d. https://it.mathworks.com/help/matlab/math/choose-an-ode-solver.html?searchHighlight=ode solver&s_tid=doc_srchtitle. (Accessed 16 December 2018).
[35] L. Di Felice, P.U. Foscolo, L. Gibilaro, CO_2 capture by calcined dolomite in a fluidized bed: experimental data and numerical simulations, Int. J. Chem. React. Eng. 9 (2011).
[36] S. Stendardo, L. Di Felice, K. Gallucci, P.U. Foscolo, CO_2 capture with calcined dolomite: the effect of sorbent particle size, Biomass Convers. Biorefinery. 1 (2011) 149–161.
[37] B.R. Stanmore, P. Gilot, Review-calcination and carbonation of limestone during thermal cycling for CO_2 sequestration, Fuel Process. Technol. 86 (2005) 1707–1743.